This document is confidential and is proprietary to the American Chemical Society and its authors. Do not copy or disclose without written permission. If you have received this item in error, notify the sender and delete all copies.

Self-Defensive Antimicrobial Surfaces Using Polymyxin-Loaded Poly(styrene sulfonate) Microgels

Journal:	ACS Biomaterials Science & Engineering	
Manuscript ID	ab-2022-00783a.R2	
Manuscript Type:	Article	
Date Submitted by the Author:	n/a	
Complete List of Authors:	Xiao, Xixi; Stevens Institute of Technology, Chemical Engineering and Materials Science Ji, Jingjing; Syracuse University, Biomedical and Chemical Engineering Wang, Haoyu; Stevens Institute of Technology, Biomedical Engineering Nangia, Shikha; Syracuse University, Biomedical and Chemical Engineering Wang, Hongjun; Stevens Institute of Technology, Biomedical Engineering Libera, Matthew; Stevens Institute of Technology, Chemical Engineering	



Self-Defensive Antimicrobial Surfaces Using Polymyxin-Loaded Poly(styrene sulfonate) Microgels

Xixi Xiao,¹ Jingjing Ji,² Haoyu Wang,³ Shikha Nangia,² Hongjun Wang,^{3,4} and Matthew Libera^{1*}

- Department of Chemical Engineering and Materials Science Stevens Institute of Technology Hoboken, NJ 07030
- Department of Biomedical and Chemical Engineering Syracuse University
 Syracuse, NY 13244
- ³ Department of Biomedical Engineering Stevens Institute of Technology Hoboken, NJ 07030
- ⁴ Center for Healthcare Innovation Stevens Institute of Technology Hoboken, NJ 07030
- * mlibera@stevens.edu corresponding author

Revised manuscript submitted to: ACS Biomaterials Science and Engineering

Keywords (4-6): Drug delivery, infection, microgel, antibiotic, complexation, contact transfer

Abstract

Self-defensive antimicrobial surfaces are of interest because they can inhibit bacterial colonization while minimizing unnecessary antimicrobial release in the absence of a bacterial challenge. One self-defensive approach uses self-assembly to first deposit a sub-monolayer coating of polyelectrolyte microgels and subsequently load those microgels by complexation with smallmolecule antimicrobials. The microgel-antimicrobial complexation strength is a key parameter that controls the ability of the antimicrobial both to remain sequestered within the microgels when exposed to medium and to release in response to a bacterial challenge. Here we study the relative complexation strengths of two FDA-approved cationic antibiotics - colistin (polymyxin E) and polymyxin B - with microgels of poly(styrene sulfonate) (PSS). These polymyxins are similar cyclic polypeptides with +5 charge at pH 7.4. However, polymyxin B substitutes an aromatic ring for a dimethyl moiety in colistin, and this aromaticity can influence complexation via π and hydrophobic interactions. Coarse-grained molecular dynamics shows that the free-energy change associated with polymyxin B/PSS complexation is more negative than that of colistin/PSS complexation. Experimentally, in situ optical microscopy of microgel deswelling shows that both antibiotics load quickly from low-ionic-strength phosphate buffer. The enhanced polymyxin B/PSS complexation strength is then manifested by subsequent exposure to flowing antibiotic-free buffer with varying NaCl concentration. Microgels loaded with polymyxin B remain stably deswollen to higher salt concentrations than do colistin/PSS microgels. Importantly, exposing loaded microgels to E. coli in nutrient-free flowing phosphate buffer shows that bacteria are killed by physical contact with the loaded microgels consistent with the contact-transfer mechanism of self-defensiveness. *In vitro* culture experiments show that these same surfaces nevertheless support the adhesion, spreading and proliferation of human fetal osteoblasts. These findings suggest a pathway to create a self-defensive antimicrobial surface effective under physiological conditions based on the non-metabolic bacterial-triggered release of FDA-approved antibiotics.

Introduction

Biomaterials-associated infection occurs when bacteria attach to the surface of a tissue-contacting biomedical device and proliferate into a biofilm.^{1, 2} The treatment of such an infection is challenging because bacteria in the biofilm state are very resistant to traditional antibiotic treatments. There can be severe complications, and the infection can often only be resolved by removing the device altogether.^{3, 4} A key intervention point to prevent device-associated infection is thus to create a surface able to avoid the initial colonization event.

One anti-colonization strategy involves self-defensive surfaces.⁵ These are able to locally release an antimicrobial when and where planktonic bacteria challenge a surface. Three bacteria-triggered release mechanisms have thus far been identified for such surfaces. Using a layer-by-layer (LbL) approach, Sukhishvili et al. reported a polyanionic hydrogel thin film that releases antibiotics in response to a local decrease in pH caused by bacterial metabolism.^{6,7} Boulmedais et al. demonstrated an LbL film constructed by chitosan and hyaluronan able to locally release an antimicrobial peptide (AMP) due to hyaluronidase secretion by metabolizing bacteria.^{8,9} More recently, we have shown that bacteria can trigger the release of cationic antimicrobials complexed within polyanionic microgels simply by bacteria-microgel contact in the absence of bacterial metabolic processes.¹⁰

Among the advantages of using polyelectrolyte microgels is the fact that they can be deposited on a complex 3-D surface to form a sub-monolayer coating by simple electrostatic self-assembly. They can subsequently be loaded by a second simple, non-line-of sight, electrostatic self-assembly step. Since the coating is sub-monolayer, a significant fraction of the underlying substrate remains exposed to interact with tissues cells in much the same manner of an unmodified substrate.

A successful self-defensive surface based on a sub-monolayer surface coating of polyelectrolyte microgels must include a number of key attributes. Among them are: (i) loading by microgel/antimicrobial complexation; (ii) sequestration (i.e., retention) of the complexed antimicrobial within the microgels; (iii) bacteria-triggered release of the antimicrobial and bacterial killing (i.e., antimicrobial behavior); and (iv) cyto/tissue-compatibility. Liang et al.¹⁰ demonstrated these characteristics using microgels of poly(acrylic acid) (PAA) complexed with a cationic antimicrobial peptide referred to as Sub5. Self-defensive behavior was attributed to contact transfer, where complexation within the bacterial envelope is favored so antimicrobial is transferred from the microgel to the bacterium when a bacterium comes in close proximity to the modified surface. More recently, Zhao et al. have used an *in vitro* model of operating room (OR) contamination to show similar behavior in PAA microgels complexed with a cationic antimicrobial peptoid (TM1).¹¹ Experiments using PAA microgels complexed with colistin, a cationic FDAapproved antibiotic active against gram-negative bacteria, also successfully demonstrated E. coli killing by bacteria/microgel contact in the absence of nutrients. However, these experiments were done in low-ionic-strength buffer. 10 In low-ionic-strength buffer and in the absence of a bacterial challenge, colistin remained sequestered in PAA for many weeks. When exposed to phosphate buffered saline (PBS) with a physiological pH of 7.4 and an ionic strength of $[Na^+] = 0.14$ M, however, colistin was very rapidly released because of the disruption of pairing between cationic colistin amine groups and anionic microgel acid groups. In short, the colistin/PAA complexation

is insufficiently strong. Self-defensive behavior by contact transfer has yet to be demonstrated under physiological conditions using an FDA-approved antibiotic.

Understanding and controlling the antibiotic/microgel complexation strength is a central element of self-defensive contact transfer. Polyelectrolyte complexation has been extensively investigated by the LbL community, 12-14 and complexation strength can be tuned by modifying the polyelectrolyte hydrophobicity, 15 aromaticity, 16, 17 and charge density. 18, 19 We have recently compared the relative complexation strengths of colistin with PAA microgels and with poly(styrene sulfonate) (PSS) microgels, 20 and both experiments and simulations show that colistin/PSS complexation is stronger than that of colistin/PAA. PAA is a weak polyelectrolyte with a pK_a of about 4.5, and PSS is a strong polyelectrolyte with a pK_a of about 1, so under physiological conditions (pH 7.4) both are negatively charged. But, importantly, the aromaticity in PSS introduces additional opportunities for hydrophobic and π interactions during complexation and creates favorable steric conditions that maximize cation-anion pairing opportunities.

Just as the microgel composition can be varied to explore complexation strength, so too can the nature of the cationic antimicrobial be varied. Here we study the relative complexation strength and self-defensive properties of two FDA-approved cationic antibiotics (Fig. 1) - polymyxin B and colistin - complexed within PSS microgels. Because their primary amines are protonated, these polymyxins are positively charged at physiological pH. They are active against gram-negative bacteria.²¹ Polymyxin B and polymyxin E (colistin) are used clinically and increasingly for the treatment of infections involving multi-drug-resistant gram-negative bacteria.^{22,23} Relative to colistin (+5, 1155 Da), polymyxin B (+5, 1203 Da) substitutes an aromatic D-phenylalanine for colistin's aliphatic D-leucine (red circles in Fig. 1).²⁴⁻²⁶ There are cationic FDA-approved antibiotics that are active against gram-positive bacteria (e.g. vancomycin), but their complexation strength with anionic microgels made of PAA or PSS appears to be

insufficiently strong to remain complexed when exposed to buffers at physiological pH and physiological ionic strength.

While colistin-loaded PAA microgels self-defensive demonstrate antimicrobial behavior against E. coli in low-ionic-strength nutrient-free buffer, the self-defensive properties of colistin/PSS and polymyxin B/PSS have not yet been studied. Here we show that both systems meet all four of the key attributes for selfdefensive behavior. Based on the differences between them, we further hypothesize that polymyxin B will complex more strongly and thus enhance the long-term sequestration behavior under physiological conditions needed for possible translation to in vivo biomedical applications.

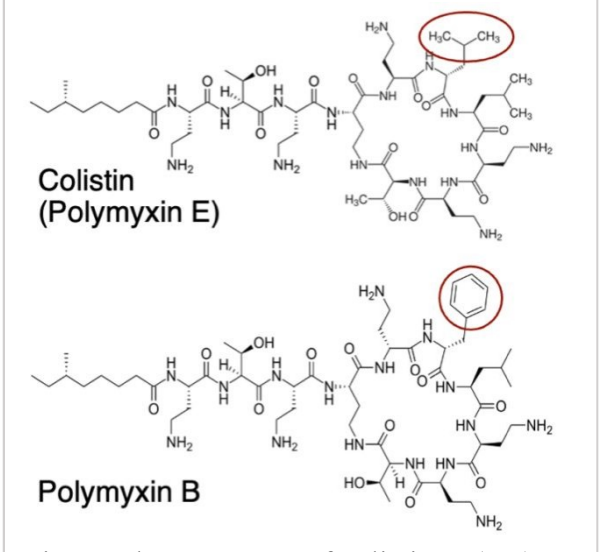


Fig. 1: The structures of colistin A (top) and polymyxin B1 (bottom) are similar except for the substitution of an aromatic ring (red circle).

Experimental Methods

Microgel Synthesis

All chemicals were purchased from Sigma-Aldrich (St. Louis, MO) and used without further purification. PSS microgels were prepared by thermal-initiated free-radical polymerization using a water-in-oil suspension following methods described previously. An aqueous precursor solution was mixed from 750 mg sodium styrene sulfonate (NaSS), 75 mg N,N'-methylene-bisacrylamide (BIS), 135 μ L 0.18 M ammonium persulfate (APS) solution, and 3 mL type I deionized (DI) water. Under N₂ gas pressure, this precursor solution was dispersed in 120 mL paraffin oil with 950 mg span 80 surfactant through a Shirasu Porous Glass (SPG) membrane with a nominal mean pore size of 5 μ m. The resulting emulsion was maintained at 65 °C under continuous N₂ bubbling for deoxygenation. After 1 h, microgels were separated from the oil via centrifugation. They were subsequently washed by repeated centrifugation and re-suspension (10x) in ethyl alcohol and then (10x) in DI water.

Polymyxin Loading and Sequestration

The antibiotic loading and sequestration were studied as described previously²⁰ by in situ optical microscopy in a continuous flow chamber (Bioptech FCS2). A pre-cleaned 40 mm diameter coverslip was treated with oxygen plasma for 3 min, exposed to 0.2 mg/mL poly(allylamine hydrochloride) (PAH) for 1 h, and then washed 3× with DI water. Microgels were deposited onto the primed coverslip by exposing the PAH-primed surface to a colloidal aqueous solution of microgels in 0.01 M phosphate buffer for 30 min and then washing with microgel-free 0.01 M phosphate buffer. This process produced a sub-monolayer coating of microgels on the transparent glass substrate. The modified coverslip was inserted into the flow chamber. A Fluigent pressurebased controller coupled with a bidirectional flow sensor was used to control the flow of buffer across the surface-bound microgels. Unless otherwise indicated, a flow rate of 100 µL/min was used. The microgels were imaged in situ using an inverted microscope (Nikon, Eclipse Ti-E) equipped with a high-sensitivity CCD Camera (pco.pixelfly series by PCO AG Kelheim, Germany) and a CFI S Fluor ELWD 20x objective lens (NA=0.45, WD = 8.2 - 6.9 mm). Brightfield images were analyzed using FIJI.^{27, 28} The microgel diameters were measured from 2D images in a direction parallel to the underlying substrate, and these diameters were normalized to the diameter of the same microgel measured in pH 7.4 low-ionic-strength (0.01 M) phosphate buffer (4 mM NaH₂PO₄, 6 mM Na₂HPO₄) whose [Na⁺] = 0.016 M. The zeta potential of the unloaded and loaded microgels suspended in phosphate buffer with $[Na^+] = 0.016$ M and $[Na^+] =$ 0.136 M was measured with a Zetasizer (Nano ZS, Malvern, UK).

The amount of loaded antibiotic was determined using calibrated UV absorption measurements. First, 100 μ L of PSS microgel suspension in DI water was placed in a 1 mL centrifuge tube and allowed to dry overnight. The weight corresponding to the dried microgels was determined by subtracting the weight of the empty tube. We assumed that the dry sulfonate monomers each included a neutralizing Na⁺ ion. The dried microgels were then exposed to 1 mL of 0.01 M phosphate buffer containing either 1 mg/mL of colistin or polymyxin B. After 24 h the tube was centrifuged and 100 μ L aliquots of the supernatant were extracted and used for UV absorbance measurements. The absorption values were converted to antibiotic concentrations

using a calibration curve determined from a series of solutions with known concentrations of either colistin sulfate or polymyxin B sulfate. This experiment was repeated 8 times.

Bacteria culturing

E. coli (New England BioLabs, C2987) were incubated in Tryptic Soy Broth (TSB) at 37 $^{\circ}$ C overnight. Prior to use, samples of *E. coli* were vortexed, centrifuged, and resuspended in sterilized 0.01 M phosphate buffer 3 times and then diluted to a final concentration of 10^8 CFU/mL. To measure their zeta potential, *E. coli* were suspended in phosphate buffer with [Na⁺] = 0.016 M or [Na⁺] = 0.136 M.

Bacteria-Triggered Antibiotic Release

Bacteria-triggered antibiotic release was studied under continuous flow of nutrient-free buffer through a PDMS reactor (Fig S1). The reactor was divided into upper and lower chambers, each with a volume of approximately 300 µL, by a membrane filter (Isopore; Millipore) with a 0.4 µm mesh size. Microgels were electrostatically deposited onto the PAH-primed glass surface and imaged in situ using a Nikon Eclipse inverted optical microscope. The microgels were subsequently loaded with either colistin or polymyxin B following the protocol described above. The as-loaded microgel diameters were measured by bright-field imaging. The microgels were then exposed to E. coli using two different experimental formats. In one (Fig. S1A), 300 µL of a bacterial suspension (108 CFU/mL) in 0.01 M phosphate buffer was injected into the lower chamber. Nutrient-free phosphate buffer with $[Na^+] = 0.016 \text{ M}$ or 0.136 M was then flowed through the chamber (20 µL/min). The bacteria were isolated in the lower chamber by the 0.4 µm membrane, and there they had direct contact with the loaded microgels. After 8 h of flow, the top chamber, the membrane, and excess buffer from the lower chamber were removed. Live/dead stain (SYTO 9/Propidium iodide (PI); Invitrogen) prepared in phosphate buffer with [Na⁺] = 0.016 M or $[Na^+] = 0.136$ M was introduced into the lower chamber to stain the E. coli there. Confocal immunofluorescence images were collected using a Nikon Eclipse Ti-E inverted microscope with a C1 confocal system and a 60x water-immersion (NA = 1.2, WD = 0.27 mm) objective lens. The bacteria were then removed, and the medium was replaced with 0.01 M phosphate buffer to enable measurement of the final microgel diameters by bright-field imaging. The second set of experiments followed an identical procedure except that the loaded microgels were deposited on the glass cover slip at the top of the upper chamber (Fig S1B). In this format, the bacteria were prevented from directly contacting the microgels by the membrane separating the two chambers.

Coarse-Grained Molecular Dynamics Simulations

Coarse-grained molecular dynamics (CG MD) was used to simulate the complexation system of antibiotic (polymyxin B) and PSS. The generation of MARTINI CG models of colistin and PSS was illustrated in our previous studies. Similarly, PyCGTOOL was used to generate the MARTINI coarse-grained model parameters of polymyxin B. The initial configuration was created by placing one PSS chain and one polymyxin B into a cubic simulation box (side length = 16 nm). The insane.py script was used to add polarizable water (PW) and Na+ for charge neutrality. The polymyxin B/PSS system was allowed to equilibrate for 2 μ s, and then steering MD simulation was performed. The simulation details closely followed our previous studies of

assessing colistin complexation with PSS and PAA.²⁰ All CG MD simulations were performed using GROMACS version 2019.³⁵ The PMF, or relative free energy ΔG , value for each system was determined using umbrella sampling (US)³⁶⁻³⁸ along a reaction coordinate, ξ . The US used a 3-step process: (1) a series of evenly distributed configurations or windows was generated along ξ ; (2) biased simulations were run at different values of ξ ; and (3) the mean force F_{ξ} at each ξ value was calculated. The maximum binding energy of a particular antibiotic molecule to a PSS molecule was then taken as the difference between the maximum and the minimum energy points in the PMF curve (ΔG vs. the distance between the center of mass of the antibiotic and PSS molecule).

Cell Culture

The cytocompatibility of surfaces modified by antibiotic-loaded PSS microgels was studied using human fetal osteoblasts (hFOB, ATCC, Virginia). hFOB cells were cultured in a 1:1 mixture of DMEM and Ham's F12 medium containing 2.5 mL L-glutamine and 10% FBS (Atlantic Biologicals) at 34 °C with 5% CO₂ and 95% humidity until 70-80% confluence. Glass coverslips were used as substrates either in the PAH-primed condition (control) or modified by polymyxin B-loaded microgels. Prior to cell culture, the samples were sterilized using 70 vol% of ethanol and autoclaved DI-water followed by UV irradiation for 20 min. Each sample was seeded with hFOB cells at a density of 5,000 cells/cm² for 15 min and subsequently incubated in 6-well plates with 2 mL medium in each well.

Cell viability, morphology, proliferation, and differentiation

Cell proliferation on various substrates (PAH-primed glass slides and polymyxin B-loaded PSS microgel-modified glass slides) was assessed by the MTS assay. Upon culture for 1, 4 and 7 days at 34°C, 20 μ L of MTS solution containing phenazine ethosulfate (PES) was added to each well and further cultured for 2 h at 34°C. Absorbance at 490 nm was recorded. A one-way ANOVA t-test was performed to test the statistical difference between different substrates.

After culture for 1, 4 and 7 days, cell viability was further evaluated by staining with the Live/Dead kit (calcein-AM and ethidium homodimer-1) following the manufacturer's protocol. In parallel, the time-resolved cell morphology was also characterized. Briefly, the culture at different time points was fixed with 4% (w/v) paraformaldehyde for 15 min and then washed three times with PBS. The fixed cells were permeabilized with 0.5% (w/v) Triton X-100 and blocked with 3% (w/v) BSA. The cell nuclei were stained with 4', 6-diamidino-2- phenylindole (DAPI, Sigma, USA), and the cell skeletal filament actin (F-actin) was stained with Alexa Fluor 488-conjugated phalloidin. The stained cells were examined with a Nikon 80i upright epifluorescence microscope, and images were recorded using NIS-ElementsBR 3.10 Software (Nikon).

The expression of selected osteogenic marker genes - specifically, type I collagen (COL-1), Runt-related transcription factor (RUNX2) and osteopontin (OPN)- in 7-day cultured cells on different substrates under the osteogenic differentiation conditions (cultured at 39.4°C with osteoinductive supplements, *i.e.*, 100 µg/mL of ascorbic acid and 10 mM of β -glycerophosphate) was studied using the reverse transcriptase polymerase chain reaction (RT-PCR) similar to a previous study.³⁹ The housekeeping gene (β -actin) was used as a control. Primers for the selected genes are listed in Table S1.

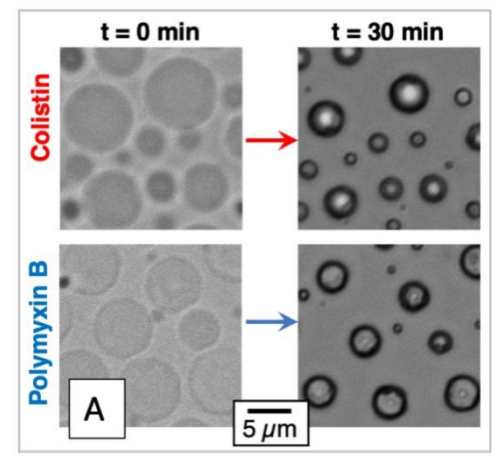
Results and Discussion

Antibiotic loading

Both colistin and polymyxin B can be loaded by complexation with PSS microgels. After deposition on glass and equilibration in 0.01 M phosphate buffer, the microgels have an average diameter of $13.7 \pm 4.9 \mu m$ (n=50 measurements). Images of the as-deposited microgels (Fig. 2A left, t=0 min) show relatively little image contrast since they are highly hydrated. Subsequent exposure to 0.01 M phosphate buffer containing 1 mg/ml of either antibiotic causes the microgels to deswell due to complexation with the antibiotic to an average normalized loaded diameter, D_L, which is some percentage of the initial unloaded diameter in 0.01 M buffer. The colistin-loaded diameter, D_{τ}^{Col} , is 52.0% and the polymyxin B-loaded diameter, D_L^{PB} , is 53.6%. In both cases, the loading process occurs over a period of about 10 min with little diameter change thereafter (Fig. 2B).

Deswelling occurs in part because the release of Na^+ counterions (5 Na^+ for each fully complexed antibiotic molecule) reduces the osmotic pressure and in part because the polyvalent nature of the antibiotics creates new non-covalent crosslinks within the microgels. Deswelling increases the polymer fraction within the microgels and leads to greater image contrast (Fig 2A top right, t = 30 min). During this process the zeta potential of the microgels changes from -40.5 mV in the unloaded state to almost neutral in the fully loaded state (Table 1).

We used calibrated UV absorption measurements to quantify the amount of loaded antibiotic. These measurements show that 0.35 ± 0.01 mg of (dry) PSS microgels loads 0.44 ± 0.05 mg of colistin or 0.47 ± 0.00 (0.0018) mg of polymyxin B. These values correspond to a molar ratio of PSS (monomer) to colistin of 4.9 and to polymyxin B of 4.7. Since each antibiotic molecule brings +5 charges, these measurements indicate almost full compensation of amine/sulfonic acid pairings due to loading of either antibiotic.



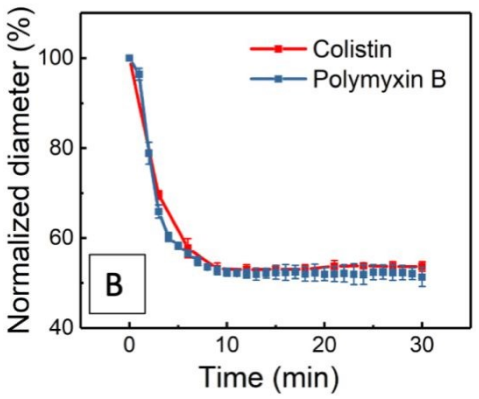


Fig. 2: Colistin and polymyxin B both load by complexation within PSS microgels. (A) *in situ* images of unloaded (top left) and loaded (top right, t=30 min) PSS microgels in 0.01 M phosphate buffer. (B) microgel diameter change during loading. Each data point/error bar correspond to the average/standard deviation of n=5 measurements. measurements.

Sequestration: Polymyxin B has a higher complexation strength

assessing the stability By of antibiotic/microgel complexation against buffer with varying ionic strength we find that polymyxin B complexes more strongly with the PSS microgels than does colistin. Fig. 3 follows the normalized microgel diameter as each type of loaded microgel is exposed to flowing phosphate buffer with $[Na^+]$ = 0.136 M. The initial diameter at t=0 min does not change when the ionic strength is increased at t = 30min to 0.136 M. Over time, however, the diameter of the colistin-loaded microgels slowly increases before leveling at 57.3%. This swelling indicates colistin release, which can be attributed to Na+ shielding of pairings between amine groups within the colistin and sulfonate groups within the PSS. As we have reported previously,²⁰ the increased [Na⁺] in the buffer by itself can affect the diameter of an unloaded PSS microgel [20], so at t=1000 min the buffer was switched to 0.01 M phosphate buffer ([Na⁺] =0.016 M) to enable a comparison to the initial unloaded diameter. The solid red triangular point at t=1030 min corresponds to a final diameter, D_{NF} , of 75.8 \pm 3.9% when equilibrated in 0.01 M buffer. This indicates that some, but not all, of the loaded colistin is released when exposed to a Na⁺ concentration typical of a physiological medium. In contrast, when exposed to an identical environment, no diameter change is observed in microgels loaded with polymyxin B. Their final normalized diameter

Table 1 - Zeta potentials					
Sample	[Na+] (M)	zeta potential (mV)			
unloaded PSS	0.016	-40.5 ± 3.4			
microgels	0.136	-28.3 ± 0.9			
Colistin-loaded microgels	0.016	0.4 ± 0.4			
	0.136	-1.7 ± 0.3			
Polymyxin B-	0.016	1.65 ± 0.3			
loaded microgels	0.136	-3.8 ± 0.6			
E coli	0.016	-33.3 ± 1.0			
	0.136	-10.5 ± 1.5			

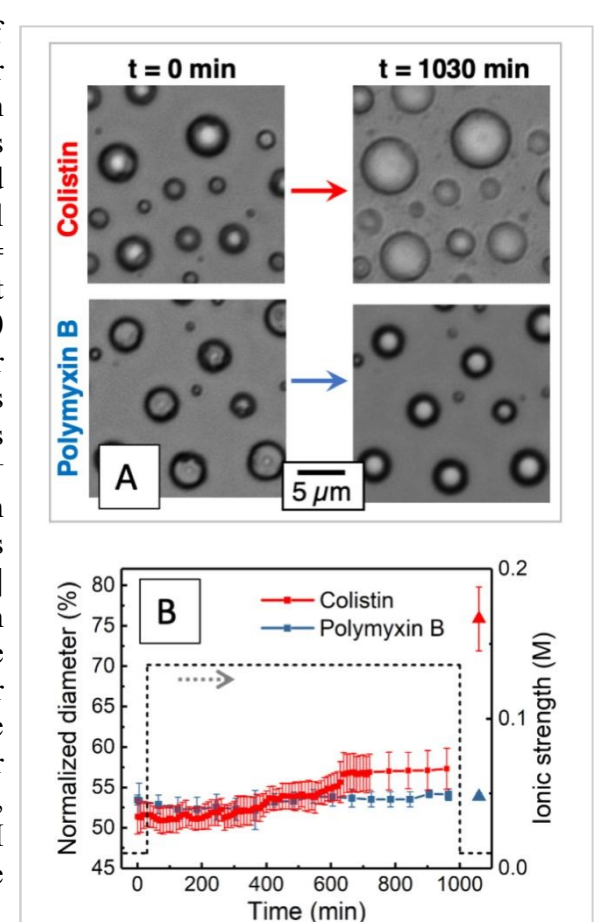


Fig. 3: (A) Images illustrating the diameter change of microgels loaded with either colistin of polymyxin B after exposure to flowing buffer with [Na⁺] = 0.136 M. (B) Normalized diameter change for loaded microgels exposed to flowing polymyxin-free phosphate buffer (dashed black line) with [Na⁺] = 0.01 M (t=0 min); 0.136 M (t=30 min); and 0.01 M (t=1000 min). The solid triangles indicate the normalized diameter at t=1030 min. Each data point/error bar corresponds to the average/standard deviation from n = 5 microgels.

in 0.01 M buffer remains at $53.8 \pm 0.4\%$, indicating no release of complexed polymyxin B. In other words, polymyxin B/PSS complexation is more resistant to decomplexation than

colistin/PSS complexation when exposed to buffer with a physiological level of salt.

Experiments such as those described by Fig. 3 were repeated using flowing buffer containing various concentrations of NaCl. In each experiment the average (n=5) as-loaded diameter, D_L , was first measured in 0.01 M phosphate buffer (e.g., t=0 in Fig. 3). These measurements give values of $D_L^{Colistin} = 52.0 \pm 1.2\%$ and $D_L^{Polymyxin\,B} = 53.6 \pm 1.1\%$. After flowing buffer with a particular [Na⁺] for 1000 min, the microgels were equilibrated in 0.01 M phosphate buffer for 30 min. and the average normalized final (NF) diameter, D_{NF} , was measured (e.g., t = 1030 min in Fig. 3). The results are tabulated in Table S2. No antibiotic release is indicated when $D_{NF} = D_L$, and full antibiotic release is indicated when $D_{NF} = 100\%$.

We converted the values of D_L and D_{NF} from Table S2 into a measure of doping in the microgels. Doping quantifies the extent to which charged polyelectrolyte acid groups are electrostatically compensated by salt cations.^{40, 41} Here a doping event corresponds to the disruption of the pairing between an amine group on a guest antibiotic molecule and a sulfonic acid group within a host microgel. We assume that the doping level, y, scales with the microgel volume:

$$y = \frac{D_{NF}^3 - D_L^3}{100^3 - D_I^3} \qquad \dots [1]$$

Figure 4 shows the [Na⁺]-dependent doping level for antibiotic-loaded microgels after soaking in flowing buffer for 1000 min. While the concentration of complexed antibiotic is not necessarily linearly related to microgel volume (eq. [1]), changing that functional dependence has little effect on the general position and shape of the curves in Fig. 4. The colistin data were reported previously²⁰ and are included here to illustrate differences between the colistin/PSS and polymyxin B/PSS systems.

Despite the fact that colistin and polymyxin B both stably complex with PSS for extended periods under conditions of low ionic strength, the doping behavior at higher salt concentrations is different. Importantly, doping (antibiotic release) in the colistin/PSS system is

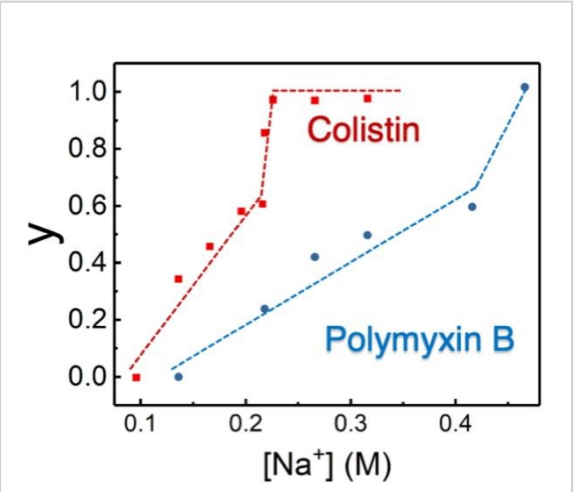


Fig. 4: Doping level (y) in colistin/PSS (red) and polymyxin B/PSS (blue) as a function of [Na⁺] in the surrounding flowing phosphate buffer. The dashed lines are added as guides to delineate different regions of doping behavior.

evident at $[Na^+] > 0.096$ M while polymyxin B/PSS remains entirely undoped (antibiotic sequestered) for the important condition of $[Na^+] = 0.136$ M. For all ionic strengths studied, $y_{polymyxin B} < y_{colistin}$. At the high-concentration extreme where y=1, the colistin/PSS system is fully doped for $[Na^+] = 0.226$ M whereas $[Na^+] = 0.466$ M is required to fully dope the polymyxin B/PSS system. Both systems undergo roughly linear doping with increasing $[Na^+]$, but the different slopes likely reflect the additional non-electrostatic contribution of the aromatic moiety in polymyxin B. Interestingly, both systems reflect a clear discontinuity in slope at higher $[Na^+]$, which may indicate

a transition where non-electrostatic interactions play a controlling role in the antibiotic/microgel complexation.

Coarse-grained molecular dynamics simulations also indicate that polymyxin B/PSS is complexation stronger than colistin/PSS complexation. Figure 5 shows the PMF profile calculated by separating a molecule of each of the two antibiotics from a PSS polymer molecule. Starting from an equilibrated antibiotic/PSS configuration, the antibiotic molecule was detached from the PSS molecule to compute the PMF profile. The ΔG corresponds to the difference between the minimum energy point along the PMF curve and the energy of the detached colistin when it reaches a separation > 4.0 nm. The same process was repeated for colistin/PSS. The calculated free-energy change for colistin/PSS is -63.8 kJ/mol, and polymyxin B/PSS is -81.3 kJ/mol indicating that the polymyxin B/PSS has the greater complexation strength.

Bacteria-triggered antibiotic release

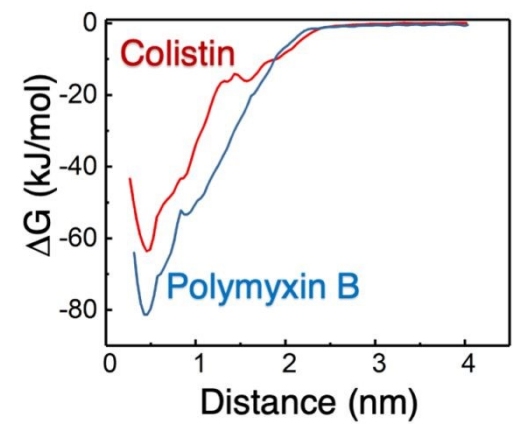


Fig. 5: Binding energies of colistin/PSS (red) and polymyxin B/PSS (blue) from steered molecular dynamics and umbrella-sampling simulations in a 0.15 M NaCl solution. The x axis represents the distance between the center of mass between a PSS polymer chain and the center of mass of the antibiotic.

Based on prior results where contact with E. coli was able to trigger the release of colistin sequestered by complexation within poly(acrylic acid) microgels, 10 here we expect that contact with E. coli should similarly trigger the release of either colistin or polymyxin B from PSS microgels. To test this hypothesis, we used a simple flow system that would either enable or prevent contact between loaded microgels and E. coli (Fig. S1). In a so-called single chamber experiment (Fig. S1A), PSS microgels were electrostatically deposited onto a PAH-primed glass coverslip that acted as the chamber bottom, and E. coli were constrained to remain within that same chamber by a 0.4 μ m mesh membrane. The microgels were either left unloaded or loaded with colistin or polymyxin B. Nutrient-free phosphate buffer with $[Na^+] = 0.016$ M or 0.136 M was flowed (20 μ L/min) through the chamber for 8 hrs. The bacteria were then exposed to live/dead stain to assess their viability.

Fig. 6 summarizes the imaging assays from the single-chamber experiments. The top row shows the control experiment where the bacteria interact with unloaded PSS microgels that were electrostatically deposited onto PAH-primed glass. The propidium iodide from the live/dead stain kit interacts with the PSS, presumably via electrostatic interaction with PSS sulfonate group and further enhanced by π interactions with the aromatic ring (such staining does not occur in unloaded PAA microgels¹⁰), so the microgels appear red. Importantly, the bacteria are almost exclusively green indicating that they survive in the nutrient-free buffer. These images correspond to projections of the 3-D confocal imaging cube, so multiple layers of bacteria can be visualized.

In clear contrast to the unloaded control experiments, identical experiments involving microgels loaded with either colistin or polymyxin B show that the majority of bacteria are dead.

Qualitatively similar killing occurs for experiments performed in both low-ionic-strength buffer ($[Na^+] = 0.016 \text{ M}$) and in physiological-strength buffer ($[Na^+] = 0.136 \text{ M}$).

The fact that some bacteria remain green, and are thus alive, in the images of Fig. 6 indicates that these bacteria did not contact a loaded microgel or did so insufficiently to drive antibiotic transfer. This surface is not necessarily optimized to have the highest killing efficiency. Engineering such a surface would likely involve smaller microgels spaced more closely together in order to maximize the probability of contact during a bacterial challenge. We further note that, because of the finite reservoir size of each microgel, these surfaces are better suited clinically relevant applications involving relatively small numbers of bacteria. These conditions, for example, are typical of contamination in the operating room (OR), and we have recently shown that titanium surfaces modified by PAA microgels loaded with antimicrobial peptoid are highly effective preventing bacterial at colonization using an in vitro model of OR contamination. 11, 42

Additional information about the bacteria-microgel interaction is given by changes in the microgel diameters.

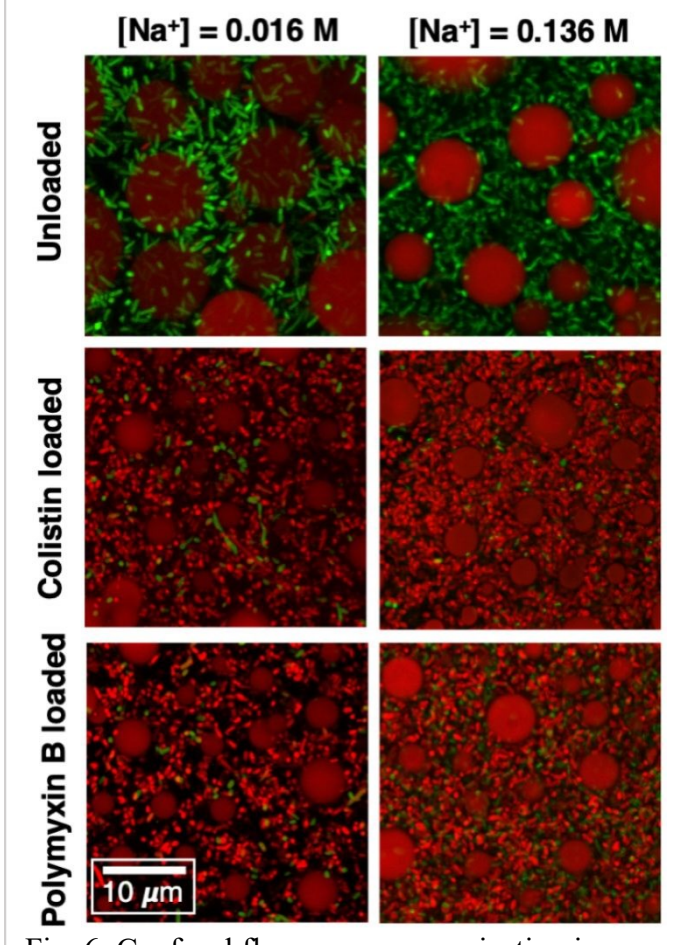


Fig. 6: Confocal fluorescence z-projection images of *E. coli* after 8 h of contact with unloaded PSS microgels (top), colistin-loaded microgels (middle), and polymyxin B-loaded microgels (bottom). The flowing medium was phosphate buffer with [Na⁺] = 0.016 M (left) or 0.136 M (right). Live = green, and dead = red.

Bacteria-induced diameter changes were assessed by comparing to reference diameters where loaded microgels were exposed to bacteria-free flowing buffer (either $[Na^+] = 0.016$ M or 0.136 M) for 8 h. The final diameter measurement was then made in the standard low-ionic strength ($[Na^+] = 0.016$ M) buffer. These reference values are given in Fig. 7 as the solid red circles. In the absence of bacteria, the fact that the microgel diameters after 8 h exposure to flowing buffer are essentially the same as the as-loaded diameters indicates that colistin remains stably complexed within the microgels (sequestered) in 0.016 M buffer and polymyxin B remains sequestered in both 0.016 M and 0.136 M buffer. Consistent with Fig. 3, exposure to bacteria-free buffer with [Na+] = 0.136 causes the release of some colistin (Fig. 7B) where the diameter (red filled circle) has increased from the as-loaded diameter of 52% to 64%.

In all four cases, however, Fig. 7 indicates that contact with *E. coli* causes an increase in microgel diameter. The blue squares in Fig. 7 correspond to the diameters after 8 h exposure to *E. coli*, removal of the *E. coli*, and then re-equilibration in the standard low-ionic-strength buffer. This diameter increase is consistent with the imaging results of Fig. 6, which indicate a preponderance of dead bacteria that must be driven by antibiotic release.

The fact that contact with the *E. coli* triggers antibiotic release is further substantiated by a control experiment that used a double-chamber flow cell (Fig. S1B). In this set of experiments, the flow cell contained E. coli but the bacteria were prevented from contacting the loaded microgels by a 0.4 µm membrane that separated the cell into an upper chamber with loaded microgels on a glass surface and a lower chamber with bacteria. The flow $[Na^+]$ conditions (rate, time, otherwise identical to the single-chamber experiments that allowed microgel-bacteria contact. After exposure to flowing buffer for 8 h, the flow cell was opened and the microgel-modified glass surface was reequilibrated in standard 0.01 M phosphate buffer. The resulting microgel diameters are given as the green triangles in Fig. 7. They correspond closely to the control diameters (red circles) which involve only buffer and no bacteria. A one-way t-test with p = 0.05indicates statistically significant differences between the experiments that allow microgel-bacteria contact and those that do not.

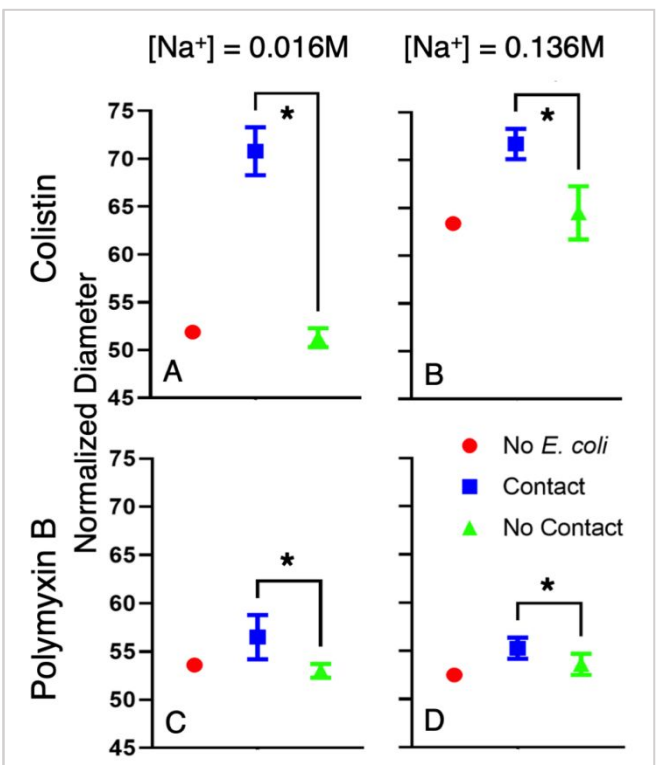


Fig. 7: Normalized microgel diameter changes indicate colistin (A, B) and polymyxin B (C, D) release triggered by $E.\ coli$ contact (blue squares) in phosphate buffer with $[Na^+] = 0.016\ M$ (left) or $0.136\ M$ (right). Each point/error bar represents the average and standard deviation from n=5 microgels. The diameter measurements were all made in $0.01\ M$ phosphate buffer. The asterisks indicate statistically significant differences (p = 0.05) when bacteria contact (blue) the loaded microgels relative to the case where that contact is prevented (green). The red circles correspond to loaded microgels exposed to bacteria-free buffer.

We attribute the triggered release of antibiotic and the subsequent killing of bacteria to the contact-transfer mechanism.^{5, 10} We can confidently rule out release triggered by local pH changes, because the flow experiments were performed using nutrient-free phosphate buffer. We can consequently expect that bacterial metabolism and any resulting changes in local pH due to the secretion of acidic metabolic products would be minimal. Similarly, we see release due to the change in ionic strength only for the case of colistin-loaded PSS at the higher salt concentration ([Na⁺] = 0.136 M). This released colistin would become quickly diluted and carried out of the flow

cell by the flowing buffer and would be very unlikely to exceed the MBC for *E. coli* that could lead to the level of killing observed by imaging (Fig. 6). Instead, we see killing and a concomitant increase in microgel diameter only when bacteria contact the loaded microgels.

Contact transfer is believed to be driven by the high concentration of negative charge and hydrophobicity associated with the bacterial cell envelope. Particularly in a gram-negative bacterium such as *E. coli*, the outer membrane contains a high concentration of lipopolysaccharides and phospholipids both of which include negatively charged phosphate moieties in addition to a high concentration of hydrophobic saturated linear acyl chains. ⁴³⁻⁴⁶ The anionic and hydrophobic properties in this outer membrane are believed to play a key role in the uptake of cationic antimicrobials where these multivalent oligocations are able to displace divalent calcium ions that electrostatically bridge liposaccharides in the outer membrane. ⁴⁷⁻⁵⁰ The contact killing mechanism first introduced by Klibanov, ⁵¹ where cationic antimicrobials covalently attached to a solid surface are able to kill bacteria, was attributed to this cationic exchange mechanism. Contact transfer is in many respects similar to contact killing. The important distinction is that the cationic antimicrobial is not covalently tethered to a substrate, so it can be transferred from host microgel to a challenging bacterium.

Zeta potential measurements support the idea that there is a thermodynamic potential able to drive transfer. Table 1 shows that the zeta potential characteristic of the loaded microgels is close to zero, as can be expected if the charge of the polyanionic microgels is fully compensated by the guest cations. In contrast, E. coli have a negative zeta potential: -33.3 mV and -10.5 mV in phosphate buffer with $[Na^+] = 0.016$ M and 0.136 M, respectively. Hence, if a bacterium comes sufficiently close to a loaded microgel, there will be a potential gradient that can drive decomplexation of the antibiotic from the microgel, its transfer from the microgel to the bacterium, and its re-complexation within the bacterial outer membrane. As we have discussed previously, ¹⁰ we can place an optics-limited upper bound of several hundred nanometers to how close a bacterium and a microgel must be for contact, but the distance is more likely to be on the order of molecular dimensions (10's of nanometers). Our double-chamber flow experiments indicate that preventing close proximity of the bacteria to the microgels prevents transfer, presumably because the potential gradient is much less steep. We furthermore note that proximity is likely to be essential for the transfer itself, because, once an antibiotic molecule decomplexes and diffuses out of its host microgel, the probability of it being carried away by the flowing medium will increase rapidly with the increasing microgel-bacterium separation. In that case, we would not observe the killing indicated by the images in Fig. 6.

We note that bacterial contact does not fully deswell the loaded microgels. None of the blue squares in Fig. 7 corresponds to 100%. We speculate that this is a consequence of the changing concentration of antibiotic complexed within the microgels. As antibiotic is released, the gradient in chemical potential between antibiotic complexed within the microgels and the same antibiotic complexed within an adjacent bacterial cell envelope would grow less until at some threshold concentration that gradient would be insufficient to drive transfer despite the proximity of the bacterium. The fact that the final diameter of the polymyxin B/PSS microgels is much less than that of the colistin/PSS microgels (blue squares in Fig. 7) is furthermore consistent with our finding that polymyxin B/PSS complexation is stronger than colistin/PSS complexation. The initial

potential gradient would be less in the polymyxin B case, and less polymyxin B would have to be released to before reaching the threshold where no further transfer could occur.

Cytocompatibility of microgel-modified surfaces

Because of its higher complexation strength and more stable sequestration within PSS microgels under physiological our cytocompatibility conditions. evaluation focused on surfaces modified by polymyxin B-loaded microgels. modified surfaces were compared to PAHprimed glass surfaces as the control. We note that exposed PAH (polycationic) will become rapidly coated by serum proteins having a net negative charge at pH 7.4 (e.g., albumin). This will occur both on the PAH -primed control surfaces and on the PAHprimer exposed between microgels on the microgel-modified surfaces. As shown in Fig. 8, the microgel-modified surfaces support the attachment and spreading of hFOB cells in a manner similar to that of the PAH-primed glass control surface for multiple time points (1, 4 and 7 days). In addition to the cell staining, we note that the microgels were also stained blue. We attribute this to DAPI interactions with polymyxin B. Live/dead staining of the culture shows essentially no dead cells (data not shown). Clearly, both the modified and control surfaces supported cell growth based on the phalloidin staining.

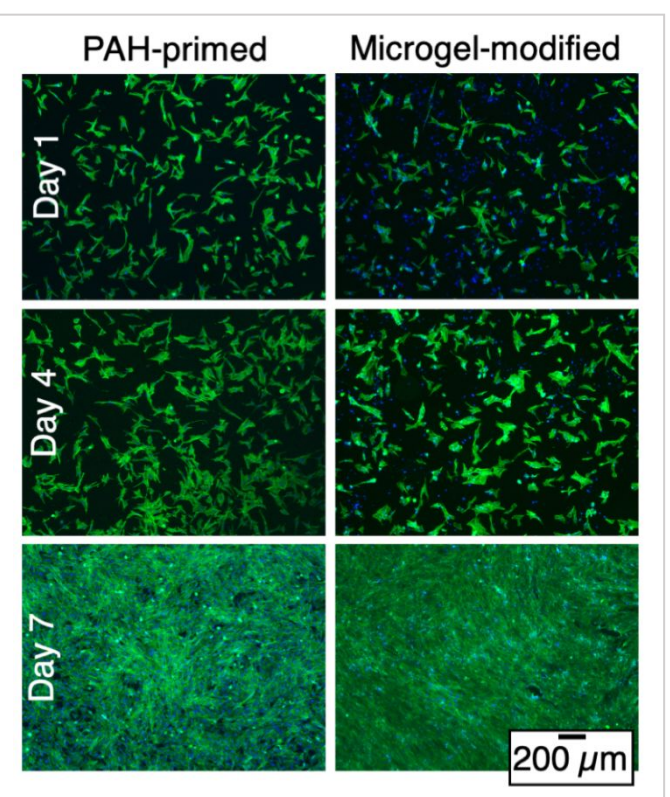


Fig. 8: hFOB cell morphology after 1, 4, 7 days of culture on PAH-primed glass (left) and polymyxin B-loaded microgel-modified glass (right). The hFOB cells were stained by DAPI (nuclei) and phalloidin (actin). Staining indicates complexation interactions between PSS microgels and DAPI (blue).

An MTS assay was also performed to quantify the cell proliferation on these surfaces (Fig. 9A). This assay indicates no statistically significant difference between the control and modified surfaces in terms of their metabolic activities, and both surfaces supported continuous cell growth. Since hFOB cells are transfected with a temperature-sensitive plasmid for better maintenance of their pluripotency, elevated temperature can induce the osteogenic differentiation.³⁹ Thus, the influence of surfaces modified by polymyxin B-loaded microgels on the osteogenesis of hFOB cells (cultured at 39.4 °C) was also studied by following the expression of representative osteogenic marker genes (COL-1, RUNX2 and OPN) via RT-PCR. Again, no significant differences were seen between PAH-primed glass and the microgel-modified surfaces (Fig. 9B). Collectively, these results indicate that surfaces modified by polymyxin B-loaded PSS microgels behave comparably to the control surfaces in terms of supporting the attachment, proliferation and differentiation of hFOB cells.

We have previously shown that hFOB cells do not trigger the release of colistin from PAA microgels.¹⁰ We see no evidence here that these cells trigger the release of polymyxin B from PSS microgels. We attribute this to the fact that charge density associated osteoblasts and many other eukaryotic cells is less than that associated with the bacterial envelope. Thus, the gradient in chemical potential induced by proximity to an osteoblast would be less than that induced by proximity to a bacterium. The fact that polymyxin B/PSS complexation is stronger than that of colistin/PAA complexation also implies that hFOB cells should not be able to trigger the release of polymyxin B. We furthermore note that, while polymyxin B is known to cause DNA damage to mammalian cells,^{52, 53} sequestering it within PSS microgels effectively cloaks it from the tissue cells and, as supported by studies, minimizes our hFOB cytotoxicity. For the same reason, we did pursue traditional hemolysis measurements to access cytocompatibility, because the antibiotics are being delivered locally in response to specific triggers (bacterial contact) rather than systemically through the blood stream.

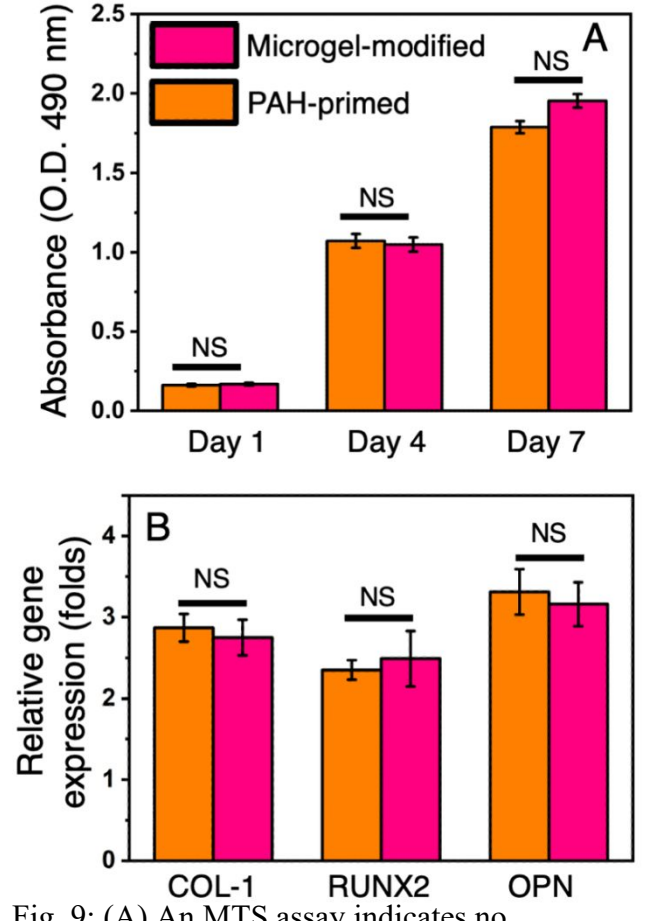


Fig. 9: (A) An MTS assay indicates no statistically significant (NS) difference in hFOB cell proliferation between cells grown on surfaces modified by polymyxin B loaded microgel-modified glass and PAH-primed glass.

(B) Gene expression of osteogenic markers against β -actin (housekeeping gene) ($n \ge 3$) in hFOBs again shows no statistically significant difference between the two surfaces.

Conclusions

We have explored the relative strength of complexation between polyanionic microgels made from poly(styrene sulfonate) PSS and two polymyxins - colistin (polymyxin E) and polymyxin B. *In situ* measurements of microgel swelling and deswelling during complexation loading and subsequent release indicate that PSS complexation with polymyxin B is stronger than that with colistin. We attribute the difference to the aromaticity in polymyxin B, which provides for additional π - π and hydrophobic interactions. This experimental finding is corroborated by calculations of complexation strength by coarsegrained molecular dynamics.

Challenging glass surfaces modified by antibiotic-loaded PSS microgels with *E. coli* leads to bacterial killing in a manner consistent with the concept of contact transfer. Our experiments

used flowing nutrient-free buffer that both minimizes the influence of possible bacterial metabolism and removes any antimicrobial eluted into the flowing medium. Live/dead staining indicates bacterial killing accompanied by microgel deswelling (antibiotic release) when *E. coli* are allowed to physically contact the loaded microgels. Short-term antimicrobial behavior is observed using both colistin and polymyxin B, though surfaces modified using polymyxin B are better suited to preserve longer-term antimicrobial behavior because of its stronger complexation with the host poly(styrene sulfonate) microgels. Significantly, these experiments were done using FDA-approved antibiotics under conditions of physiological pH and ionic strength, which indicates that the PSS/polymyxin system is a good candidate for possible translation towards clinical use.

Supporting Information Available

The following files are available free of charge:

Figure S1 schematically illustrates the flow chamber used to permit or prevent contact between E. coli and antibiotic-loaded PSS microgels.

Table S1 summarizes the primers used for RT-PCR

Table S2 provides values of DNF for various salt concentrations used to calculate Fig. 4.

Acknowledgements

The Stevens portion of this work was supported by the Army Research Office (W911NF2010277) and by the NIDDK Diabetic Complications Consortium (RRID:SCR_001415, www.diacomp.org), grants DK076169 and DK115255. The computational component of the work was completed at Syracuse University through resources provided by Information and Technology (Eric Sedore, Larne Pekowsky, and Michael R. Brady) as well as by the Extreme Science and Engineering Discovery Environment (XSEDE), which is supported by National Science Foundation grant number ACI-1053575. Collaborative aspects of the work were supported in part by an NSF ERC Planning Grant (NSF #1936926) and an NSF GCR Grant (NSF # 2219014).

References

- 1. Arciola, C. R.; Campoccia, D.; Montanaro, L., Implant infections: adhesion, biofilm formation and immune evasion. *Nature Reviews Microbiology* **2018**, *16* (7), 397-409.
- 2. Bryers, J. D., Medical biofilms. *Biotechnol Bioeng* **2008**, *100* (1), 1-18.
- 3. David M, P.; Douglas R, O.; Michael R, K.; Arlen D, H., Delayed Reimplantation Arthroplasty for Candidal Prosthetic Joint Infection: A Report of 4 Cases and Review of the Literature. *Clinical Infectious Diseases* **2002**, *34* (7), 930-938.
- 4. Inzana, J. A.; Schwarz, E. M.; Kates, S. L.; Awad, H. A., Biomaterials approaches to treating implant-associated osteomyelitis. *Biomaterials* **2016**, *81*, 58-71.
- 5. Xiao, X.; Zhao, W.; Liang, J.; Sauer, K.; Libera, M., Self-defensive antimicrobial biomaterial surfaces. *Colloids Surf B Biointerfaces* **2020**, *192*, 110989.
- 6. Albright, V.; Zhuk, I.; Wang, Y.; Selin, V.; van de Belt-Gritter, B.; Busscher, H. J.; van der Mei, H. C.; Sukhishvili, S. A., Self-defensive antibiotic-loaded layer-by-layer coatings: Imaging of localized bacterial acidification and pH-triggering of antibiotic release. *Acta Biomater* **2017**, *61*, 66-74.
- 7. Pavlukhina, S.; Lu, Y.; Patimetha, A.; Libera, M.; Sukhishvili, S., Polymer Multilayers with pH-Triggered Release of Antibacterial Agents. *Biomacromolecules* **2010**, *11* (12), 3448-3456.
- 8. Cado, G.; Aslam, R.; Séon, L.; Garnier, T.; Fabre, R.; Parat, A.; Chassepot, A.; Voegel, J. C.; Senger, B.; Schneider, F.; Frère, Y.; Jierry, L.; Schaaf, P.; Kerdjoudj, H.; Metz-Boutigue, M. H.; Boulmedais, F., Self-Defensive Biomaterial Coating Against Bacteria and Yeasts: Polysaccharide Multilayer Film with Embedded Antimicrobial Peptide. *Advanced Functional Materials* **2013**, *23* (38), 4801-4809.
- 9. Séon, L.; Lavalle, P.; Schaaf, P.; Boulmedais, F., Polyelectrolyte Multilayers: A Versatile Tool for Preparing Antimicrobial Coatings. *Langmuir* **2015**, *31* (47), 12856-12872.
- 10. Liang, J.; Wang, H.; Libera, M., Biomaterial surfaces self-defensive against bacteria by contact transfer of antimicrobials. *Biomaterials* **2019**, *204*, 25-35.
- 11. Zhao, W.; Wang, H.; Xiao, X.; De Stefano, L.; Katz, J.; Lin, J. S.; Barron, A. E.; Schaer, T. P.; Wang, H.; Libera, M., Peptoid-Loaded Microgels Inhibit the Colonization of Titanium Rods by Staphylococci in an in vitro Model of Operating-Room Contamination. *Advanced Materials Interfaces* **2022**, *early view 2201662*.
- 12. Borges, J.; Mano, J. F., Molecular interactions driving the layer-by-layer assembly of multilayers. *Chemical Reviews* **2014**, *114* (18), 8883-8942.

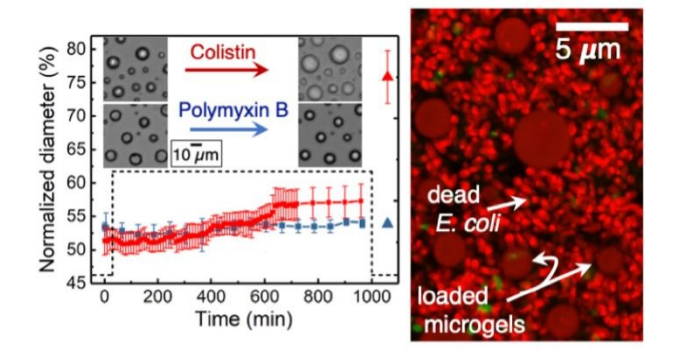
- 13. Fu, J.; Fares, H. M.; Schlenoff, J. B., Ion-Pairing Strength in Polyelectrolyte Complexes. *Macromolecules* **2017**, *50* (3), 1066-1074.
- 14. Yang, M.; Shi, J.; Schlenoff, J. B., Control of Dynamics in Polyelectrolyte Complexes by Temperature and Salt. *Macromolecules* **2019**.
- 15. Sadman, K.; Wang, Q.; Chen, Y.; Keshavarz, B.; Jiang, Z.; Shull, K. R., Influence of Hydrophobicity on Polyelectrolyte Complexation. *Macromolecules* **2017**, *50* (23), 9417-9426.
- 16. Fan, H.; Wang, J.; Tao, Z.; Huang, J.; Rao, P.; Kurokawa, T.; Gong, J. P., Adjacent cationic-aromatic sequences yield strong electrostatic adhesion of hydrogels in seawater. *Nat Commun* **2019**, *10* (1), 5127.
- 17. Kim, S.; Yoo, H. Y.; Huang, J.; Lee, Y.; Park, S.; Park, Y.; Jin, S.; Jung, Y. M.; Zeng, H.; Hwang, D. S.; Jho, Y., Salt Triggers the Simple Coacervation of an Underwater Adhesive When Cations Meet Aromatic pi Electrons in Seawater. *ACS Nano* **2017**, *11* (7), 6764-6772.
- 18. Chang, L. W.; Lytle, T. K.; Radhakrishna, M.; Madinya, J. J.; Velez, J.; Sing, C. E.; Perry, S. L., Sequence and entropy-based control of complex coacervates. *Nat Commun* **2017**, *8* (1), 1273.
- 19. Sing, C. E., Development of the modern theory of polymeric complex coacervation. *Adv Colloid Interface Sci* **2017**, *239*, 2-16.
- 20. Xiao, X.; Ji, J.; Zhao, W.; Nangia, S.; Libera, M., Salt Destabilization of Cationic Colistin Complexation within Polyanionic Microgels. *Macromolecules* **2022**, *55* (5), 1736-1746.
- 21. Satlin, M. J.; Jenkins, S. G., Polymyxins. **2017**, 1285-1288.e2.
- 22. Nang, S. C.; Azad, M. A. K.; Velkov, T.; Zhou, Q. T.; Li, J., Rescuing the Last-Line Polymyxins: Achievements and Challenges. *Pharmacol Rev* **2021**, *73* (2), 679-728.
- 23. Velkov, T.; Roberts, K. D.; Thompson, P. E.; Li, J., Polymyxins: a new hope in combating Gram-negative superbugs? *Future Medicinal Chemistry* **2016**, *8* (10), 1017-1025.
- 24. Kwa, A.; Kasiakou, S. K.; Tam, V. H.; Falagas, M. E., Polymyxin B: Similarities to and differences from colistin (polymyxin E). *Expert Review of Anti-Infective Therapy* **2007**, *5* (5), 811-821.
- 25. Velkov, T.; Thompson, P. E.; Nation, R. L.; Li, J., Structure-activity relationships of polymyxin antibiotics. *Journal of Medicinal Chemistry* **2010**, *53* (5), 1898-1916.
- 26. Yin, J.; Meng, Q.; Cheng, D.; Fu, J.; Luo, Q.; Liu, Y.; Yu, Z., Mechanisms of bactericidal action and resistance of polymyxins for Gram-positive bacteria. *Applied Microbiology and Biotechnology* **2020**, *104* (9), 3771-3780.

- 27. Schindelin, J.; Arganda-Carreras, I.; Frise, E.; Kaynig, V.; Longair, M.; Pietzsch, T.; Preibisch, S.; Rueden, C.; Saalfeld, S.; Schmid, B.; Tinevez, J.-Y.; White, D. J.; Hartenstein, V.; Eliceiri, K.; Tomancak, P.; Cardona, A., Fiji: an open-source platform for biological-image analysis. *Nature Methods* **2012**, *9*, 676.
- 28. Schneider, C. A.; Rasband, W. S.; Eliceiri, K. W., NIH Image to ImageJ: 25 years of image analysis. *Nature Methods* **2012**, *9*, 671.
- 29. Graham, J. A.; Essex, J. W.; Khalid, S., PyCGTOOL: Automated Generation of Coarse-Grained Molecular Dynamics Models from Atomistic Trajectories. *Journal of Chemical Information and Modeling* **2017**, *57* (4), 650-656.
- 30. de Jong, D. H.; Singh, G.; Bennett, W. F. D.; Arnarez, C.; Wassenaar, T. A.; Schäfer, L. V.; Periole, X.; Tieleman, D. P.; Marrink, S. J., Improved Parameters for the Martini Coarse-Grained Protein Force Field. *Journal of Chemical Theory and Computation* **2013**, *9* (1), 687-697.
- 31. Marrink, S. J.; Risselada, H. J.; Yefimov, S.; Tieleman, D. P.; de Vries, A. H., The MARTINI Force Field: Coarse Grained Model for Biomolecular Simulations. *The Journal of Physical Chemistry B* **2007**, *111* (27), 7812-7824.
- 32. Monticelli, L.; Kandasamy, S. K.; Periole, X.; Larson, R. G.; Tieleman, D. P.; Marrink, S.-J., The MARTINI Coarse-Grained Force Field: Extension to Proteins. *Journal of Chemical Theory and Computation* **2008**, *4* (5), 819-834.
- 33. Periole, X.; Marrink, S. J., The Martini coarse-grained force field. *Methods Mol Biol* **2013**, 924, 533-65.
- 34. Wassenaar, T. A.; Ingólfsson, H. I.; Böckmann, R. A.; Tieleman, D. P.; Marrink, S. J., Computational Lipidomics with insane: A Versatile Tool for Generating Custom Membranes for Molecular Simulations. *Journal of Chemical Theory and Computation* **2015**, *11* (5), 2144-2155.
- 35. Abraham, M. J.; Murtola, T.; Schulz, R.; Páll, S.; Smith, J. C.; Hess, B.; Lindahl, E., GROMACS: High performance molecular simulations through multi-level parallelism from laptops to supercomputers. *SoftwareX* **2015**, *1-2*, 19-25.
- 36. Kästner, J., Umbrella sampling. *WIREs Computational Molecular Science* **2011**, *1* (6), 932-942.
- 37. Torrie, G. M.; Valleau, J. P., Monte Carlo free energy estimates using non-Boltzmann sampling: Application to the sub-critical Lennard-Jones fluid. *Chemical Physics Letters* **1974**, *28* (4), 578-581.
- 38. Torrie, G. M.; Valleau, J. P., Nonphysical sampling distributions in Monte Carlo free-energy estimation: Umbrella sampling. *Journal of Computational Physics* **1977**, *23* (2), 187-199.

- 39. Yen, M. L.; Chien, C. C.; Chiu, I. M.; Huang, H. I.; Chen, Y. C.; Hu, H. I.; Yen, B. L., Multilineage differentiation and characterization of the human fetal osteoblastic 1.19 cell line: A possible in vitro model of human mesenchymal progenitors. *Stem Cells* **2007**, *25* (1), 125-131.
- 40. Schlenoff, J. B.; Yang, M.; Digby, Z. A.; Wang, Q., Ion Content of Polyelectrolyte Complex Coacervates and the Donnan Equilibrium. *Macromolecules* **2019**, *52* (23), 9149-9159.
- 41. Yang, M.; Digby, Z. A.; Schlenoff, J. B., Precision Doping of Polyelectrolyte Complexes: Insight on the Role of Ions. *Macromolecules* **2020**, *53* (13), 5465-5474.
- 42. Zhao, W.; Libera, M.; Prysak, M.; Katz, J.; De Stefano, L., An in vitro model of microbial contamination in the operating room. *Journal of Biomedical Materials Research Part B Applied Biomaterials* **2022**, *110*, 2472-2479.
- 43. Ebbensgaard, A.; Mordhorst, H.; Aarestrup, F. M.; Hansen, E. B., The role of outer membrane proteins and lipopolysaccharides for the sensitivity of escherichia coli to antimicrobial peptides. *Frontiers in Microbiology* **2018**, *9* (SEP).
- 44. May, K. L.; Grabowicz, M., The bacterial outer membrane is an evolving antibiotic barrier. *Proceedings of the National Academy of Sciences of the United States of America* **2018**, *115* (36), 8852-8854.
- 45. Nikaido, H., Molecular Basis of Bacterial Outer Membrane Permeability Revisited. *Microbiology and Molecular Biology Reviews* **2003**, *67* (4), 593-656.
- 46. Silhavy, T. J.; Kahne, D.; Walker, S., The bacterial cell envelope. *Cold Spring Harbor perspectives in biology* **2010**, *2* (5).
- 47. Akhoundsadegh, N.; Belanger, C. R.; Hancock, R. E. W., Outer membrane interaction kinetics of new polymyxin B analogs in Gram-negative bacilli. *Antimicrobial Agents and Chemotherapy* **2019**, *63* (10).
- 48. Herce, H. D.; Garcia, A. E., Cell penetrating peptides: How do they do it? *Journal of Biological Physics* **2007**, *33* (5-6 SPECL.ISSUE), 345-356.
- 49. Yeaman, M. R.; Yount, N. Y., Mechanisms of antimicrobial peptide action and resistance. *Pharmacol Rev* **2003**, *55* (1), 27-55.
- 50. Yount, N. Y.; Yeaman, M. R., Peptide antimicrobials: Cell wall as a bacterial target. In *Annals of the New York Academy of Sciences*, Blackwell Publishing Inc.: 2013; Vol. 1277, pp 127-138.
- 51. Tiller, J. C.; Liao, C. J.; Lewis, K.; Klibanov, A. M., Designing surfaces that kill bacteria on contact. *Proceedings of the National Academy of Sciences of the United States of America* **2001**, 98 (11), 5981-5985.

- 52. Yun, B.; Zhang, T.; Azad, M. A. K.; Wang, J.; Nowell, C. J.; Kalitsis, P.; Velkov, T.; Hudson, D. F.; Li, J., Correction to: Polymyxin B causes DNA damage in HK-2 cells and mice (Archives of Toxicology, (2018), 92, 7, (2259-2271), 10.1007/s00204-018-2192-1). *Archives of Toxicology* **2018**, *92* (7), 2273-2274.
- 53. Yun, B.; Zhang, T.; Azad, M. A. K.; Wang, J.; Nowell, C. J.; Kalitsis, P.; Velkov, T.; Hudson, D. F.; Li, J., Polymyxin B causes DNA damage in HK-2 cells and mice. *Archives of Toxicology* **2018**, *92* (7), 2259-2271.

Table of Contents Graphic



Supporting information

Self-Defensive Antimicrobial Surfaces Using Polymyxin-Loaded Poly(styrene sulfonate) Microgels

Xixi Xiao, ¹ Jingjing Ji, ² Haoyu Wang, ³ Shikha Nangia, ² Hongjun Wang, ³ and Matthew Libera ^{1*}

¹ Department of Chemical Engineering and Materials Science Stevens Institute of Technology

Hoboken, NJ 07030

² Department of Biomedical and Chemical Engineering

Syracuse University

Syracuse, NY 13244

³ Department of Biomedical Engineering

Stevens Institute of Technology

Hoboken, NJ 07030

 $* \ mlibera@stevens.edu$

corresponding author

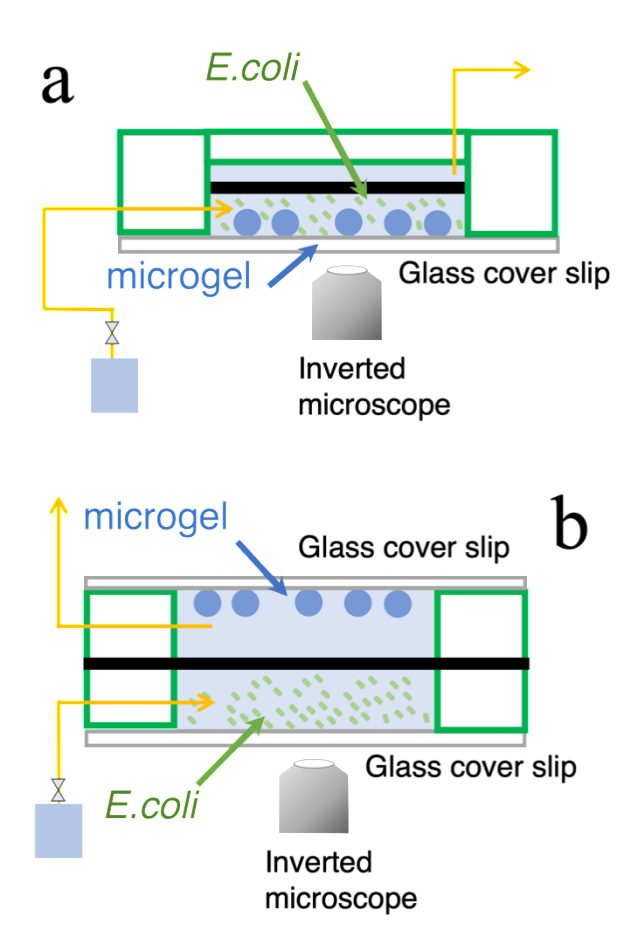


Figure S1: Schematic illustrations of the flow systems to (A) enable or (B) prevent contact between antibiotic-loaded microgels and *E. coli*.

Calculation of 8 hours No E. coli

The diameter changes of colistin/polymyxin B loaded-microgel in *E. coli*-free phosphate buffer were observed using the experimental setup illustrated in Fig S2a. The antibiotic-loaded microgel-modified surfaces were exposed to flowing phosphate buffer following the concentration change depicted by the dashed line in Fig S2b. Microgel diameter was measured every 5 hours in 0.016 M [Na+] phosphate buffer. (Colistin-loaded microgel = red, polymyxin B-loaded microgel = blue).

The 8 hours flowing data was estimated based on the linear relationship of microgel diameter change after 5 hours, 10 hours, and 15 hours flowing in phosphate buffer with 0.136 M [Na+]. The standard deviation was calculated based on 95% confidence interval (red/blue dash line in Fig 2Sc, d).

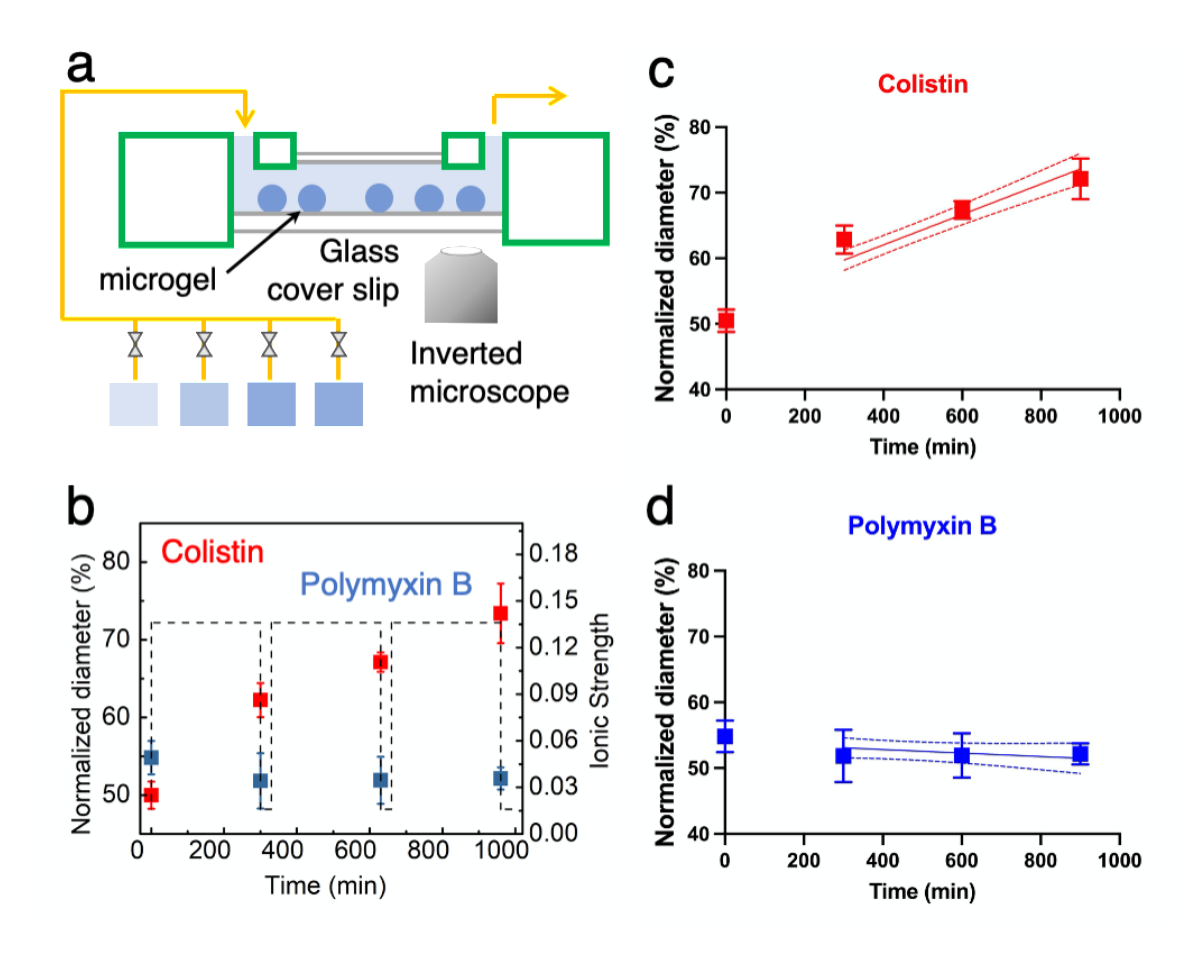


Figure S2: a) Schematic illustration of the flow system to follow microgel-buffer interactions, b) Antibiotic-loaded PSS microgel respond to phosphate buffer with varying [Na+], c,d) Colistin (polymyxin B) -loaded PSS microgel respond to 0.136 M [Na+], dash lines represent calculated error bar based on 95% confidence interval.

Table S1: Primer sequences used for gene expression analysis via reverse transcription polymerase chain reaction (RT-PCR).

Gene	5' - 3'	Primer sequence
β-Actin	Sense	5'-AACCCTAAGGCCAACCGTG-3'
	Antisense	5'-CAGGATTCCATACCCAAGAAG-3'
COL-1	Sense	5'-TCTCCACTCTTCTAGTTCCT-3'
	Antisense	5'-TTGGGTCATTTCCACATGC-3'
RUNX2	Sense	5'-CGTGGCCTTCAAGGTGGTAG-3'
	Antisense	5'-GAGGCATTCCGGAGCTCAG-3'
OPN	Sense	5'-ACATCCAGTACCCTGATGCTACAG-3'
	Antisense	5'-TGGCCTTGTATGCACCATTC-3'

Calculation of doping level

The doping level is calculated using equation 1:

$$y = \frac{D_{!"}^{\#} - D_{\$}^{\#}}{100 - D_{\$}^{\#}}$$

Where the normalized diameter (D_{NF}) of antibiotics-loaded PSS microgel after flowing with a phosphate buffer with varying [Na+] are listed in Table S1. the diameter of PSS microgel after loading with colistin is $D_{\$}^{\%\&')^*(+} = 52.0 \pm 1.1$, after polymyxin B loading is $D_{\$}^{-\&'\cdot/\cdot0(+1)} = 53.7 \pm 1.1$.

Table S2 - Average and standard deviation (n=5) of the microgel diameter after exposure to flowing phosphate buffer with varying [Na+] for 1000 min and then equilibrated in 0.01 M phosphate buffer (D_{NF}).

[Na ⁺] (M)	D _{! "}	D _{! "} *\$%+,+-&) /
0.096	51.9 ± 1.7	No data
0.136	75.9 ± 3.9	52.5 ± 1.8
0.166	81.7 ± 1.8	No data
0.196	86.2 ± 2.5	No data
0.216	87.2 ± 2.2	70.2 ± 1.2
0.218	95.0 ± 1.7	No data
0.226	99.9 ± 0.7	No data
0.266	99.1 ± 2.3	79.5 ± 1.7
0.316	99.3 ± 2.6	80.8 ± 1.3
0.416	No data	86.8 ± 0.3
0.516	No data	100.5 ± 0.9